CHALMERS
UNIVERSITY OF TECHNOLOGY

High speed driving stability of road vehicles under crosswinds: an aerodynamic and vehicle dynamic parametric sensitivity analysis

VEHICLE SYSTEM DYNAMICS
https://doi.org/10.1080/00423114.2021.1903516

High speed driving stability of road vehicles under crosswinds: an aerodynamic and vehicle dynamic parametric sensitivity analysis

Adam Brandt [a,b], Bengt Jacobson [a] and Simone Sebben [a]

[a]Department of Mechanics and Maritime Sciences, Chalmers University of Technology, Gothenburg, Sweden; [b]CEVT (China Euro Vehicle Technology), Gothenburg, Sweden

ABSTRACT

Crosswinds affect vehicle driving stability and their influence increase with driving speed. To improve high speed driving stability, interdisciplinary research using unsteady aerodynamics and vehicle dynamics is necessary. The current demands of faster development times require robust virtual methods for assessing stability performance in early design phases. This paper employs a numerical one-way coupling between the two disciplines and uses a variety of realistic crosswind gust profiles for the aerodynamic simulations to output representative forces and moments on three vehicle dynamic models of different fidelity levels, ranging from a one-track model to a full multi-body dynamic model of a sports utility vehicle. An investigation on required model fidelity was conducted along with a sensitivity study to find key aerodynamic and vehicle dynamic characteristics to minimise the yaw velocity and lateral acceleration response during crosswinds. Transient aerodynamic simulations were used to model crosswind gusts at high speeds. Analysis of the forces and moments showed that rapid changing gusts generate overshoots in the yaw moment, due to the phase delay of the flow between the front and rear of the vehicle. A methodology for modelling this phase delay is proposed. The response of the vehicle was captured equally well by the enhanced model (mid-level fidelity) and the full multi-body dynamic model, while the simplest one-track model failed to emulate the correct vehicle response. The sensitivity study showed the importance of the positioning of the centre of gravity, the aerodynamic coefficient of yaw moment, wheel base, vehicle mass and yaw inertia. In addition, the axles' side force steer gradients and other suspension parameters revealed potential in improving crosswind stability.

ARTICLE HISTORY
Received 17 September 2020
Revised 17 December 2020
Accepted 1 March 2021

KEYWORDS
Aerodynamics; vehicle dynamics; driving stability; crosswind; high speed; parametric study; SUV

Abbreviations

CFD	Computational fluid dynamics
CoG	Centre of gravity
CP	Centre of pressure

CONTACT Adam Brandt adam.brandt@chalmers.se
This article has been republished with minor changes. These changes do not impact the academic content of the article.

SUV	Sports utility vehicle
QS	Quasi-steady (aerodynamic model)
QSD	Quasi-steady with axle delay (aerodynamic model)
tCFD	Transient CFD (aerodynamic simulation technique)
SBES	Stress-blended eddy simulation
RANS	Reynolds-averaged Navier–Stokes
DES	Detached eddy simulation
MBD	Multi-body dynamic
DoF	Degree of freedom
NSP	Neutral steering point
w_y	Crosswind velocity, m/s
w_y^{start}	Initial amplitude of crosswind gust, m/s
$w_y^{\max}$	Maximum amplitude of crosswind gust, m/s
$w_y^{\min}$	Minimum amplitude of crosswind gust, m/s
w_y^{end}	Ending amplitude of crosswind gust, m/s
t	Time, s
t_b	Gust profile build-up time, s
t_p	Gust profile pausing time, s
t_d	Gust profile drop time, s
ψ	Flow angle, deg
y^+	Non-dimensional wall distance
L	Wheel base, m
l_f	CoG to front axle distance, m
l_r	CoG to rear axle distance, m
h	CoG height above ground, m
h_{fRC}	Front axle roll centre height, m
h_{rRC}	Rear axle roll centre height, m
δ_f	Front axle steering angle, rad
δ_r	Rear axle steering angle, rad
m	Vehicle mass, kg
J_z	Yaw moment of inertia, kg/m^2
J_s	Sprung body roll moment of inertia, kg/m^2
k_{fRC}	Front axle roll stiffness, Nm/rad
k_{rRC}	Rear axle roll stiffness, Nm/rad
d_{fRC}	Front axle roll damping, Nm/(rad/s)
d_{rRC}	Rear axle roll damping, Nm/(rad/s)
F_S	Aerodynamic side force, N
F_L	Aerodynamic lift force, N
M_x	Aerodynamic roll moment, Nm
M_y	Aerodynamic pitch moment, Nm
M_z	Aerodynamic yaw moment, Nm
F_{flz}	Front left tire normal force, N
F_{frz}	Front right tire normal force, N
F_{rlz}	Rear left tire normal force, N
F_{rrz}	Rear right tire normal force, N

F_{fyw}	Front axle lateral tire force, N
F_{ryw}	Rear axle lateral tire force, N
$\hat{a}_y$	Lateral acceleration amplitude, m/s^2
$\hat{\omega}_z$	Yaw velocity amplitude, deg s
Y	Combined measure (proxy for driving stability performance)
a_y	Lateral acceleration, m/s^2
ω_z	Yaw velocity, deg/s
c_{ym}	Aerodynamic yaw moment coefficient
F_{sf}	Aerodynamic front axle side force, N
F_{sr}	Aerodynamic rear axle side force, N
Δt	Time delay between front and rear axle, s
v_x	Vehicle velocity, m/s
CC_y	Normalised tire lateral cornering stiffness
t_{gust}	Gust duration, s
w_x	Longitudinal wind velocity, m/s
V_{mag}	Flow magnitude, m/s

1. Introduction

When driving on the road, the driver's ability to control the vehicle is partly affected by external crosswind disturbances. Crosswind disturbances are, in principle, always present on open roads and their influence on the driving stability increases at higher vehicle speeds. In general, a low lateral and yaw motion response to crosswinds is desirable and will minimise the needed steering corrections by the driver [1–3]. A typical passenger vehicle has the centre of pressure (CP) located in front of the neutral steering point (NSP) [1,4], as in Figure 1. Since the NSP defines where a lateral force can be applied without producing a yaw rotation, this implies that a crosswind flow would turn the vehicle away from the wind, making it aerodynamically unstable. This underlying unstable property of passenger vehicles complicates the engineering of stable vehicles at high speeds and poses a challenge for the automotive industry. Safety, the perceived level of control and expected comfort in modern cars are reasons for the increased research focus on vehicle handling coupled to unsteady aerodynamics. Many studies available in the literature compare the effects of different aerodynamic features and investigate how to numerically couple aerodynamics and vehicle dynamics in a virtual environment [5–8]. However, few studies have investigated which aerodynamic and vehicle dynamic design parameters affect the sensitivity to crosswinds the most.

Unsteady flow conditions on the road are caused by the turbulence in the natural wind, flow disturbances by other vehicles and obstacles at the roadside [9]. Experimental studies have shown that the on-road turbulence affects the aerodynamics of vehicles significantly and that high turbulence intensities of up to 15% were seen in freeway traffic [10–12]. Moreover, a previous study [3] found that changes in crosswind magnitude often coincided with instances of perceived stability issues. The reproducibility of on-road crosswind experiments can be improved by utilising test track facilities with fans to control the external crosswind conditions [1,13–15]. To standardise experiments at these facilities, the International Standard ISO 12021:2010 [16] was formulated. The guidelines in the ISO 12021:2010 standard include a methodology where a vehicle is driven at 100 km/h into a

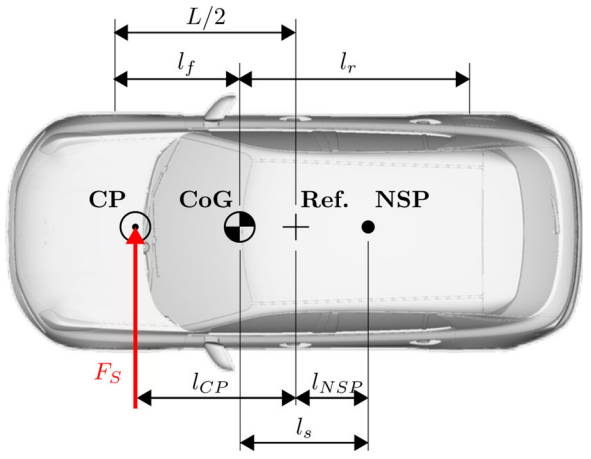

Figure 1. Top view of a vehicle visualising the longitudinal positions of the aerodynamic centre of pressure (CP), the centre of gravity (CoG), a geometric reference point midway between the axles (Ref.) and the neutral steering point (NSP).

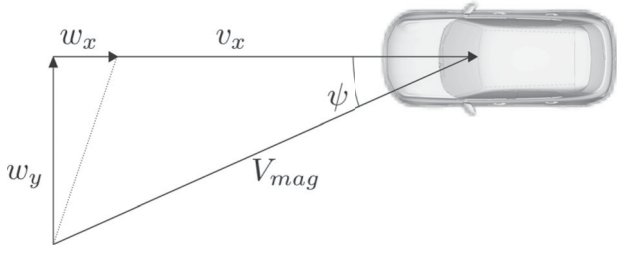

Figure 2. Schematics of how the flow angle, ψ, and flow velocity, V_{mag}, relate to the vehicle velocity, v_x, and horizontal wind components, w_x and w_y.

zone of 20 m/s crosswind, resulting in a relative flow angle of $\psi = 35.8^\circ$ (Figure 2 shows how the vehicle velocity, v_x, and horizontal wind components, w_x and w_y, affect the relative flow magnitude, V_{mag}, and angle, ψ). The resulting crosswind gust profile has been adopted in several numerical studies of crosswind sensitivity [5–8,17]. These extreme winds of 20 m/s create high aerodynamic forces and a distinct motion response of the vehicle, useful for measuring differences between vehicles and configurations. However, it has also been shown that these crosswinds are too extreme to represent most real driving scenarios [3,10–12,18,19], and are more likely investigations of extreme crosswind sensitivity, rather than driving stability performance at high speed. For example, when conducting on-road measurements of crosswind gusts in Germany, Theissen and Wojciak [18,19] found that the typical magnitude of the crosswind resulted in flow angles between 2 and 10 ° and that a zero-crossing of the flow angle occurred in 72% of the gusts. Similar results have been seen in other studies [3,20].

The aerodynamic response to a crosswind gust can be modelled or simulated in many ways. Jarlmark [21,22] and later Juhlin [23,24] created inverse dynamics models to estimate the aerodynamic load on the vehicles while driving. This was done by measuring the wind, motion of the vehicle and driver response. The inverse simulations could thus

enable an approximate solution without using full-scale windtunnels with crosswind excitation abilities. Since such windtunnel facilities are rare, much research has been focused on using computational fluid dynamics (CFD) simulations to model the transient aerodynamic loads during the crosswind gust event [5–8,14,15,17,25]. The loads can be coupled to vehicle dynamic simulations, to find the vehicle motion response to the gust. Some researchers suggest that a one-way coupling is sufficiently accurate for passenger vehicles [5,6], while another study opted for the necessity of a two-way coupling [8]. In a one-way coupling, the only interaction between the sub-fields is the aerodynamic load (forces and moments) input to the vehicle dynamic simulation. However, a more authentic description would also include the vehicle motion synchronously in the aerodynamic simulation; as in a two-way coupling. For high vehicles (buses and trucks), the necessity of two-way coupled simulations has been shown in [6,26].

The quasi-steady approach is yet another way to approximate the aerodynamic loads during a crosswind gust. This approach uses tabled data of averaged force and moment coefficients at different flow angles. From this, an interpolant can be created, which estimates the aerodynamic response based on the flow angle and magnitude. Hence, data from conventional windtunnels (or CFD) can be used with this approach. The drawback with the approach is that the transient aerodynamic effects during crosswinds are neglected; effects that were shown to be significant, at least for a simple radiused box geometry, in a study by Chadwick et al. [27]. Huemer et al. [28] altered the quasi-steady approach by including magnification coefficients of the forces' and moments' crosswind gust amplitudes together with variable time delays between the aerodynamic forces and moments. They found that an increase in the aerodynamic yaw moment amplitude caused the highest degradation of driving stability, followed by increases in aerodynamic side force and roll moment. Additionally, the time delay between the force and moment peaks showed a significant non-linear effect on driving stability. Similarly, an important aspect of driving into crosswinds is that there is a time delay between the crosswind flow at the front and rear of the vehicle, causing overshoots in the aerodynamic yaw moment, as discussed by Chadwick et al. [27].

The effect of the aerodynamic loads on the vehicle motion depends on the vehicle dynamic properties. Early analytical work used a static stability index to conclude that it was preferable to move the centre of gravity (CoG) forward, decrease the yaw mass moment of inertia and to have a positive aerodynamic pitch moment [29]. The pitch moment conclusion was later confirmed in experimental work by Howell and Le Good [30] where a strong correlation between increased pitch and improved subjective ratings was found. In 1990, MacAdam et al. [1] conducted a full-scale experimental parametric study, using seven vehicle configurations altering the positions of the aerodynamic centre of pressure (CP), CoG and varying the roll stiffness. In agreement with previous studies, they found that moving CoG forwards was beneficial. Furthermore, moving CP forwards and reducing the roll stiffness decreased the stability performance.

Even though later parametric studies also highlight the high sensitivity of the CoG [17,31–33] and the importance of the CP position relative to the NSP [33], little is still known on the influence of suspension and other vehicle properties on crosswind sensitivity. The desired positioning of CoG can conflict with other vehicle attributes and changes to the suspension kinematics and compliance might be more realistic improvements for crosswind stability. As seen, few studies have investigated the vehicle dynamic design parameters

for crosswind sensitivity and none have, to the best of the authors' knowledge, included kinematics and elasto-kinematic parameters of the wheel suspension. Furthermore, the level of fidelity needed in the vehicle dynamics model to virtually assess crosswind sensitivity is unknown. The purpose of this research is, thus, to elaborate on the required fidelity level and to perform an extensive parametric sensitivity study to gain knowledge about the most significant vehicle dynamic design parameters in comparison and synergy with aerodynamic parameters. Moreover, different methods of modelling the aerodynamic response were evaluated. Two methods using quasi-steady models, where one accounted for the phase delay between the axles, were compared to transient CFD simulations.

2. Aerodynamic methodology

The aerodynamic forces and moments are affected by the vehicle speed and the external wind conditions. This study investigates high speed driving stability at $v_x = 160$ km/h, with perpendicular crosswind disturbances of ± 5 m/s amplitude. Three crosswind gust profiles were adopted in the study, where the first two were implemented according to results found in a previous experimental study [3], while the third resembles the resulting profile from the ISO12021:2010 standard, although at the same lower amplitude of 5 m/s. The parameter values in Table 1 were used with Equation (1) [3] to generate the crosswind gusts seen in Figure 3. Profiles 1 and 2 were chosen for investigating the effects of different build-up times, t_b, and drop times, t_d, for gust profiles including a zero-crossing of the flow angle. The third profile does not include the zero-crossing, but has a fast build-up time and longer pausing time, t_p, and thus a higher integral of the crosswind velocity.

Table 1. Crosswind gust profile parameter values applied in Equation (1).

	w_y^{start} [m/s]	w_y^{max} [m/s]	w_y^{min} [m/s]	w_y^{end} [m/s]	t_b [s]	t_p [s]	t_d [s]	$t_{gust} = 2t_b + 2t_p + t_d$ [s]
Profile 1	0	5	−5	0	0.5	0	0.6	1.6
Profile 2	0	5	−5	0	0.7	0	0.2	1.6
Profile 3	0	5	5	0	0.3	0.5	0	1.6

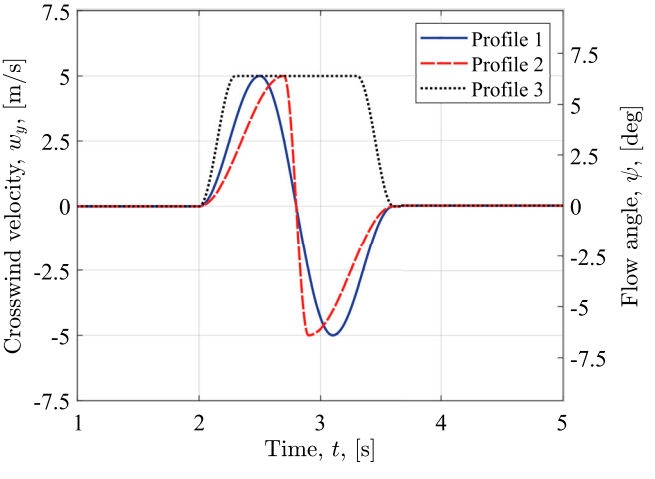

Figure 3. The three crosswind gust profile velocities, w_y, and corresponding flow angles, ψ, at 160 km/h.

The corresponding flow angle can be seen on the secondary y-axis in Figure 3. The crosswind gusts were defined in the time domain since a fixed vehicle speed was used, making the gust lengths equal. The gust duration, t_{gust}, of 1.6 s corresponds to 16 vehicle lengths, which lies in the critical range for vehicle dynamic crosswind stability reported in previous works [9,18,19].

$$
\boldsymbol{w_y(t)}\begin{cases}
= w_y^{\mathbf{start}} \\
\quad \text{for } t < t_0 \\
= w_y^{\mathbf{start}} + \dfrac{w_y^{\max} - w_y^{\mathbf{start}}}{2}\left(1 - \cos\left(\dfrac{\pi}{t_b}(t - t_0)\right)\right) \\
\quad \text{for } t_0 < t < t_0 + t_b \\
= w_y^{\max} \\
\quad \text{for } t_0 + t_b < t < t_0 + t_b + t_p \\
= w_y^{\max} - \dfrac{w_y^{\max} - w_y^{\min}}{2}\left(1 - \cos\left(\dfrac{\pi}{t_d}\left(t - t_0 - t_b - t_p\right)\right)\right) \\
\quad \text{for } t_0 + t_b + t_p < t < t_0 + t_b + t_p + t_d \\
= w_y^{\min} \\
\quad \text{for } t_0 + t_b + t_p + t_d < t < t_0 + t_b + 2t_p + t_d \\
= w_y^{end} + \dfrac{w_y^{\min} - w_y^{\mathbf{end}}}{2}\left(1 + \cos\left(\dfrac{\pi}{t_b}\left(t - t_0 - t_b - 2t_p - t_d\right)\right)\right) \\
\quad \text{for } t_0 + t_b + 2t_p + t_d < t < t_0 + 2t_b + 2t_p + t_d \\
= w_y^{\mathbf{end}} \\
\quad \text{for } t > t_0 + 2t_b + 2t_p + t_d
\end{cases} \tag{1}
$$

The test object used in the study was a compact sports utility vehicle (SUV), see Figure 4. The underbody and engine bay of the virtual model were fully detailed, while the 235/50 R19 tires were modelled as slicks.

Figure 4. A rendered image of the test vehicle used in the numerical study.

The aerodynamic forces acting on the vehicle during the crosswind gust can be estimated using various methods. This paper applied three methods, where all utilise a one-way coupling to the vehicle dynamic models:

(1) A **Quasi-steady (QS)** approach uses tabled data of time-averaged aerodynamic loads at a range of set flow angles to create a linear interpolant. The averaged load data originated from unsteady CFD simulations at constant flow angles. The interpolant function determines the aerodynamic response during the crosswind gust, based on the instantaneous flow angle and magnitude.
(2) A **Quasi-steady with axle delay (QSD)** approach extends QS by accounting for the effect of the time delay between the front and rear axle when driving into a gust ($\Delta t = \frac{L}{v_x}$). The yaw moment and side force were split up into front and rear side forces. The lift force and pitch moment were split up into front and rear lift. The roll contribution was split equally between the axles. This per-axle formulation enabled the phase shift of the aerodynamic response, e.g. the yaw moment:

$$M_z(t) = \frac{L}{2}\left(F_{sf}(t) - F_{sr}(t - \Delta t)\right) \tag{2}$$

(3) A **transient CFD (tCFD)** approach simulates the full crosswind gust events twice via a transient inlet condition. Each gust was simulated twice (with different starting times of the gust) to increase the reliability of the transient solution by making an average of the forces and moments at each time step.

2.1. CFD boundary conditions

The computational domain used in all aerodynamic modelling approaches can be seen in Figure 5(a). The wheels were modelled using rotating walls and the ground with a moving wall boundary condition of the vehicle velocity of 160 km/h. The crosswinds were prescribed with the y-component of the flow at the velocity inlet (left), while the x-component corresponded to the vehicle velocity. The quasi-steady approaches used a fixed inlet crosswind velocity while the transient CFD approach had a user-defined time-dependent function of the three gust profiles. Since two of the profiles changed sign during the gust event, it was preferred to define them at the inlet and let the flow transport the crosswinds over the domain using periodic side boundaries. The top of the domain used a symmetry boundary condition.

2.2. CFD mesh and numerical approach

The CFD mesh was adapted for crosswind simulations, by widening the refinement zones after the vehicle, see the tapered zones in Figure 5(c) along with the other refinement zones near the vehicle. The prism layer creation was done adaptively by the solver. The adaption was based on the flow around the vehicle in a steady-state solution at zero flow angle. The boundary cells were split until the target of $y^+ < 1$ was reached. This resulted in an average of 17 prism layers on the exterior and a final mesh of 200 million cells. Two views of the final mesh and near wall prism layers can be seen in Figures 5(b) and 5(c). The same mesh was used for all aerodynamic modelling approaches.

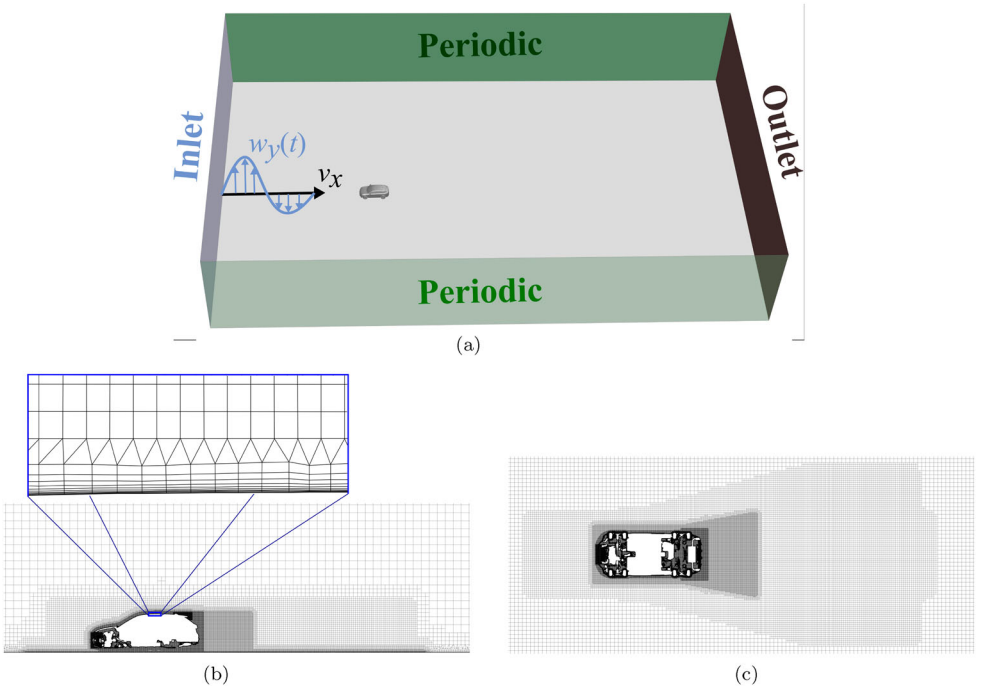

Figure 5. The CFD domain and mesh setup: (a) the computational domain, (b) section of the mesh at $y = 0$, (c) section of the mesh at axle height.

All simulations were performed using the stress-blended eddy simulation (SBES) turbulence model [34] in the commercial finite volume solver ANSYS Fluent 2020R1. The SBES model is designed with a stronger shielding of the RANS region and a faster transition to the LES region, compared with other DES models, making it more accurate for separating flows [34]. A second-order implicit temporal discretisation scheme with a time step size of $2.5 \cdot 10^{-4}$ s was used, corresponding to a temporal resolution of 406 time steps of the freestream to travel the length of the vehicle. A study by Ekman et al. [35] found this temporal resolution adequate when using the SBES model. Four inner iterations were performed at each time step, allowing the residuals to converge well below 10^{-3}. A pressure-velocity coupled Green–Gauss node based spatial discretisation was used with second-order pressure and bounded central differencing momentum schemes. The turbulent kinetic energy and specific dissipation rate used first-order discretisation, regarded sufficient since these equations are source dominated. These solver settings were used for all aerodynamic modelling approaches. The simulations were initiated using steady-state solutions. Then, the unsteady settings were gradually adjusted to reach their final values at 2 s, when the gusts were initiated at the inlet for the tCFD approach and the averaging of 1 s started for the tabulated data used in the QS/QSD approaches.

3. Vehicle dynamic methodology

3.1. Model fidelity

Vehicle dynamic models are used to enable virtual assessment of vehicle response in various driving scenarios. The models must, therefore, be representative of the real vehicle and have

sufficient fidelity (accuracy) to emulate the vehicle response. The most accurate models are the detailed multi-body dynamics (MBD) models, where kinematic and elasto-kinematic effects of the chassis, suspension and steering systems are modelled as one complex system. As a result, the MBD models use the suspension and steering components' positions (hardpoints) as input for building the model; thus, defining the model on a low hierarchical level. These complex models are often said to be of high fidelity. However, due to their complexity, high-fidelity models can be more difficult to interpret than models of lower fidelity. Moreover, vehicle requirements are set on a system level, a higher hierarchy compared to the hardpoint defined models. Hence, this becomes a drawback when trying to analyse the sensitivity of system properties, since multiple properties change when altering the hardpoints in the high-fidelity models. A viable alternative is to use the models defined on a system level, such as the bicycle model. Although they present lower fidelity, their inherent definition makes them useful when assessing system properties and finding suitable requirement settings. Additionally, the models of lower fidelity are generally more interpretable, giving more insight in the dynamics of the system, and can be used earlier in the vehicle design process when hardpoint details are still not defined. Despite their many advantages, when lower fidelity models are preferred, the issue of accuracy still needs to be addressed.

The accuracy of the lower fidelity models must be balanced with their complexity. Too little detail and the models cannot emulate the correct vehicle response anymore. Too much detail and the models lose their interpretability. Therefore, this paper examines two system-level models of low- and mid-fidelity. The low-fidelity model was used to exemplify when the model is too simple for its purpose of assessing driving stability in crosswind conditions. The mid-fidelity model incorporates enough complexity to accurately emulate the response of the high-fidelity model, within certain tolerances. This setup provided knowledge about the necessary level of model complexity for assessing straight-line driving stability. Moreover, the mid-fidelity model could be used for the parametric sensitivity study, where system properties can be varied independently.

3.1.1. Classical bicycle model (low fidelity)

The classical bicycle one-track model was used for comparison, as the low-fidelity model, in this study. The model has 2 degrees of freedom (DoF): lateral and yaw motion. The tires were modelled linearly with a lateral cornering stiffness coefficient, linearised around the static axle loads.

3.1.2. Enhanced model (mid fidelity)

The enhanced model was based on the bicycle model, but several additional vehicle properties were implemented to increase its accuracy for assessing driving stability at high speed. It was found that including a roll DoF improved the model (in line with the conclusions of a previous study on the effects of roll dynamic for crosswind sensitivity [17]). The lateral tire cornering stiffness was modelled, based on the normal load, using a second-order polynomial. The polynomial was fitted to experimental tire data. Furthermore, the enhanced model accounted for kinematic and elasto-kinematic steering effects in the suspension system. Figure 6(a) shows a schematic view of the enhanced model.

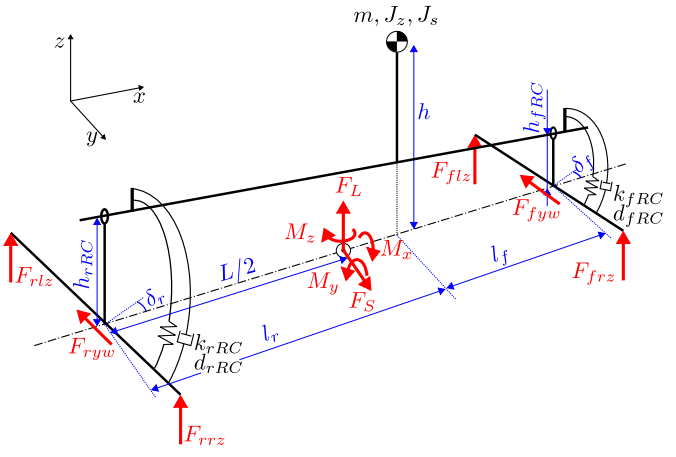

Figure 6. Schematics of the mid- and high-fidelity models: (a) the enhanced model (mid fidelity), including the aerodynamic input and (b) the high fidelity model; a multi-body dynamic model built in Adams/Car software.

3.1.3. Multi-body dynamic model (high fidelity)

A multi-body dynamic model was used as the reference model. The model can be seen in Figure 6(b). It was built in Adams/Car, using the *PAC2002* [36] (Pacejka Magic Formula) tire model and had a Gruebler count of 2136 (approximate degrees of freedom).

3.2. Model validation

The models were compared in a fidelity analysis and the enhanced model was validated using real-world data from a test-track study [3]. Further details about the test track and instrumentation setup can be found in [3]. Thirteen instances of experienced stability issues were selected from the data set. The measured vehicle motion response during the events was compared to the modelled response, where the vehicle-local wind measurements were converted to aerodynamic inputs using the quasi-steady approach.

3.3. Driver modelling

A simple driver model was used in all three vehicle dynamic models. The driver model had a locked steering angle, which was calculated to yield zero yaw velocity and lateral acceleration prior to the gust events.

4. Parametric design of experiments and analysis methodology

A design of experiments methodology was used to perform the parametric sensitivity study of the vehicle dynamic parameters in the enhanced model.

The final assessment of high speed stability in vehicle development is often done by experienced drivers at test tracks, and their subjective judgement has proven reliable and reproducible. However, their subjective assessment cannot directly be used in the virtual environment. Instead, several studies have established strong correlations between poor

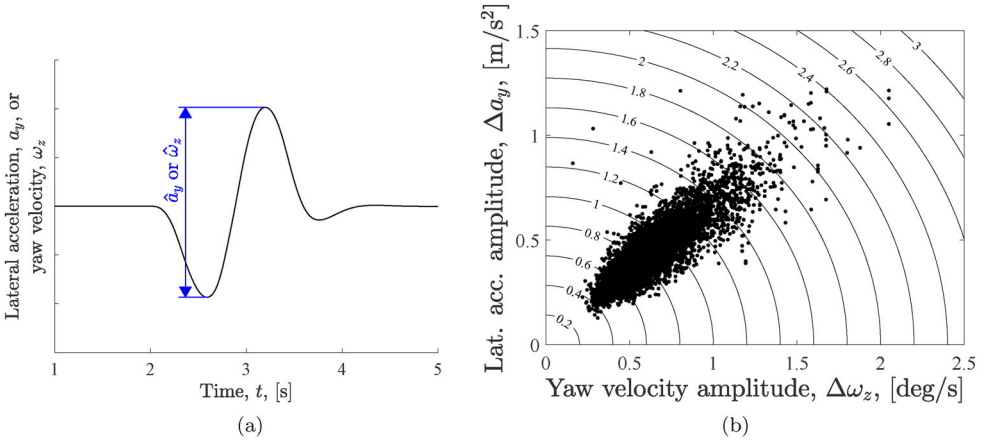

Figure 7. Description of the objective measure, Y: the proxy for driving stability performance. (a) Description of the amplitude measurement of lateral acceleration and yaw velocity. (b) The response amplitudes for a set of experimental data [3], with the objective measure (Equation 3) visualised as contour lines.

Table 2. Parameters and their intervals investigated in the sensitivity study.

No.	Parameter	Abbr.	Unit	Max – Min
V1	Wheel base	whlB	m	0.40
V2	Track width	trkW	m	0.30
V3	Centre of gravity height	CoGz	m	0.40
V4	Centre of gravity position, l_f/L	CoGx	1	0.15
V5	Vehicle mass	mass	kg	1200
V6	Sprung mass moment of inertia (x)	inertx	kgm^2	350
V7	Mass moment of inertia (z)	inertz	kgm^2	2000
V8	Normalised tire lateral cornering stiffness	corStif	1/rad	10.0
V9	Side force steer, front	sStrFr	deg/kN	0.16
V10	Side force steer, rear	sStrRe	deg/kN	0.06
V11	Roll steer, front	rStrFr	deg/deg	0.11
V12	Roll steer, rear	rStrRe	deg/deg	0.07
V13	Roll centre height, front	rcFr	m	0.14
V14	Roll centre height, rear	rcRe	m	0.14
V15	Roll stiffness, front	rStifFr	Nm/deg	1800
V16	Roll stiffness, rear	rStifRe	Nm/deg	1500
A1	Side force coefficient gradient	side	1/deg	0.025
A2	Front lift coefficient at zero flow angle	fLift0	1	0.100
A3	Front lift coefficient quadratic increase	fLiftq	$1/deg^2$	0.001
A4	Rear lift coefficient at zero flow angle	rLift0	1	0.150
A5	Rear lift coefficient increase at 1.25 deg	rLift1	1	0.010
A6	Rear lift coefficient increase at 3.75 deg	rLift3	1	0.070
A7	Rear lift coefficient increase at 7.5 deg	rLift7	1	0.060
A8	Roll moment coefficient gradient	roll	1/deg	0.003
A9	Yaw moment coefficient gradient	yaw	1/deg	0.005

subjective assessment and high variations in particularly yaw velocity and lateral acceleration [1–3]. Therefore, this study combined the amplitudes of these motions in a proxy measure for stability performance. The amplitude measurement is visualised in Figure 7(a). The combined measure utilises an elliptic formulation of the amplitudes, see Equation (3), where $\hat{a}_y$ $[m/s^2]$ and $\hat{\omega}_z$ [deg/s] were the configuration's amplitude measure for lateral

acceleration and yaw velocity, respectively.

$$Y = \sqrt{2\hat{a}_y^2 + \hat{\omega}_z^2} \tag{3}$$

Figure 7(b) shows the amplitude responses from an experimental data set [3] together with the combined objective measure. The axes show the amplitude measures while the contour lines indicate the value of the objective measure calculated using Equation (3). The figure also shows the strong correlation between lateral acceleration and yaw velocity. The measure is designed to promote a low response for both vehicle motions.

4.1. Parameters

The sensitivity study included both vehicle dynamic and aerodynamic parameters. The 16 vehicle dynamic parameters are marked with the prefix V in Table 2, and the nine aerodynamic parameters have the prefix A. The table shows the parameters' name, abbreviation, unit and investigated interval sizes between the minimum and maximum values. The nominal values were based on the existing vehicle and the intervals have been selected from existing specifications and feasible spread in parameters for multiple vehicle types. Parameters V1–V7 capture the primary vehicle dynamic properties, such as wheel base (V1) and mass (V5). V8 is the input to the polynomial modelling the tire lateral cornering stiffness. The parameter value is approximately in the same magnitude as the resulting normalised tire lateral cornering stiffness, CC_y (e.g. V8 $= 25\frac{1}{rad} \Rightarrow CC_y = 18.1\frac{1}{rad}$ at an axle load of 10,000 N). The resulting axle cornering stiffness depend on CC_y and the normal load. Parameters V9–V16 are associated with suspension characteristics, a.k.a. kinematics and compliance (K&C) parameters. Side force steer (V9–V10) account for the additional steering of the suspension and steering kinematics when side axle loads are applied, while the roll steer (V11–V12) does the same for the vehicle roll angle. The roll centre heights (V13–V14) and roll stuffiness (V15–V16) were also included as the final vehicle dynamic parameters.

The nine aerodynamic parameters were based on yaw sweep curves, where the aerodynamic coefficients of side force, roll moment and yaw moment often show a linear dependency on the flow angle. Hence, the A1, A8 and A9 parameters represent the linear gradient of the three quantities, respectively. The coefficient of front lift was modelled using two parameters, the first (A2) controlled the smallest value of front lift (at 0 deg flow angle), and the last (A3) controlled the quadratic increase of the coefficient at higher flow angles. Similarly, the coefficient of rear lift was controlled with four parameters, where the first (A4) controlled the smallest value of rear lift and the following (A5–A7) controlled the increase at higher flow angles. This modelling method of approximating the yaw sweep curves was only used in the parametric study to be able to evaluate their influence on crosswind stability. Otherwise, the exact yaw sweep curves were used in the quasi-steady approaches.

4.2. Design of experiments and parametric analysis

The initial approach evaluated a fractional factorial design of 513 design configurations (one centre point) of the vehicle dynamic parameters. However, the results showed strong non-linearity and synergies between parameters. Therefore, it was decided to use a more space-filling algorithm that enables the use of a surface response methodology. The Latin

hypercube sampling, with a maximisation of the minimum distance between design points was used. A total of 15,000 configurations were simulated, distributed between four parametric studies.

The first study investigated the vehicle dynamic parameters, while keeping the aerodynamics at constant nominal values. This investigation included 3000 configurations (1000 per gust profile). The second study focused on the aerodynamics, while keeping the vehicle dynamic parameters constant. This study also included 3000 configurations. The third and largest study included 6000 configurations since all vehicle dynamic and aerodynamic parameters were investigated simultaneously. The final study focused on the tire and suspension vehicle dynamic parameters (V8–V16). This was done since changing primary vehicle parameters (e.g. wheel base and centre of gravity position) most likely would be an unrealistic solution to improve crosswind stability. This study included 3000 design configurations.

The commercial optimisation software ModeFRONTIER 2017R5 was used to generate the Latin hypercube sampling, calculate the significant main effects (with a 95% confidence level using *t*-distribution) and to create the response surfaces used to analyse the synergy effects. The response surfaces were based on radial basis functions.

5. Results

5.1. Aerodynamic forces and moments

Figures 8(a–c) display the aerodynamic side force, yaw moment and roll moment response, respectively. The figures present comparisons between the three crosswind gust profiles and between the three aerodynamic response modelling methods: quasi-steady (QS), quasi-steady with axle delay (QSD) and transient CFD (tCFD). The tCFD results were filtered through a 32-Hz low-pass filter, to improve visibility. As can be seen in Figure 8(a), there seems to be little difference in the side force response between the modelling methods (thin, thick and dashed lines). Both quasi-steady approaches neglect any transient fluid dynamic effects, and since the transient CFD (which account for those effects) showed similar results, it could be concluded that no significant transient effect of the side force is present during crosswind gusts of the magnitude and time interval investigated in this study. Furthermore, the modelling of the time delay between the axles had a small effect on the side force results (thick and dashed lines in Figure 8a).

The axle delay modelling had a more substantial effect on the yaw moment response (Figure 8b). Note especially the positive peak overshoot at 2.75 s of QSD profile 3 (black dashed) and the negative peak of QSD profile 2 (red dashed) at 3.4 s. These effects can be explained by the observation that in constant crosswind flow, the front axle side force work to turn the vehicle away from the crosswind (increasing the aerodynamic yaw moment), while the rear axle side force work in the opposite direction for the yaw moment, as demonstrated by Theissen [19]. The positive yaw moment overshoot at 2.75 s was hence a result of high front axle side force without any counteracting side force at the rear axle. The effect at 3.4 s is even more significant since the rapid change in flow angle resulted in a brief instance when the front and rear axle side force worked together to decrease the yaw moment to its negative peak value. This effect could be confirmed by the tCFD, which also showed a negative peak at 3.4 s and an overall better agreement with the QSD solution. Moreover,

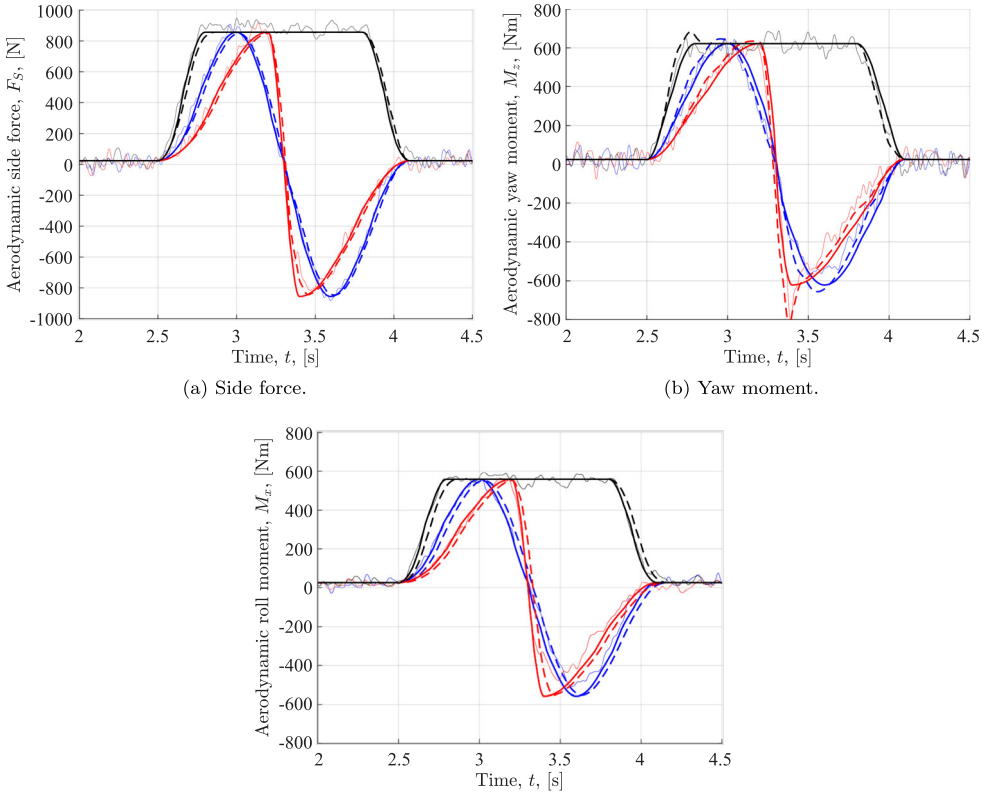

(a) Side force. (b) Yaw moment.

(c) Roll moment.

Figure 8. The aerodynamic response for gust profile 1 (**blue**), profile 2 (**red**) and profile 3 (**black**), comparing tCFD (thin lines) to QS (thick lines) and QSD (thick dashed lines) approaches. (a) Side force. (b) Yaw moment. (c) Roll moment.

this also indicated that there was no significant transient fluid dynamic effect for the yaw moment either.

The aerodynamic roll moment responses can be seen in Figure 8(c). Similar to the side force, the axle delay had a small effect on the roll moment results. The transient CFD results agreed well with the quasi-steady approaches during the positive flow angles, but had lower peak values after the change of flow direction in profiles 1 and 2. This effect is not understood, and no explanation was found in the literature.

In summary, neither the aerodynamic side force nor yaw moment showed any transient fluid dynamic effects at these crosswind magnitudes and gust time intervals. Therefore, the QSD approach was regarded as an acceptable approximation of the aerodynamic response in this study. The overshoots of the aerodynamic yaw moment could be explained by the time delay between the front and rear axle when driving into crosswinds. Thus increased aerodynamic yaw moment admittance with increased gust frequencies could be results of axle delay rather than a fluid dynamic hysteresis effect.

5.2. Fidelity analysis and model validation using experimental data

The vehicle motion response to the gust profiles (using the QSD approach) was compared for the three vehicle dynamic models of varying fidelity, see Figure 9. The multi-body

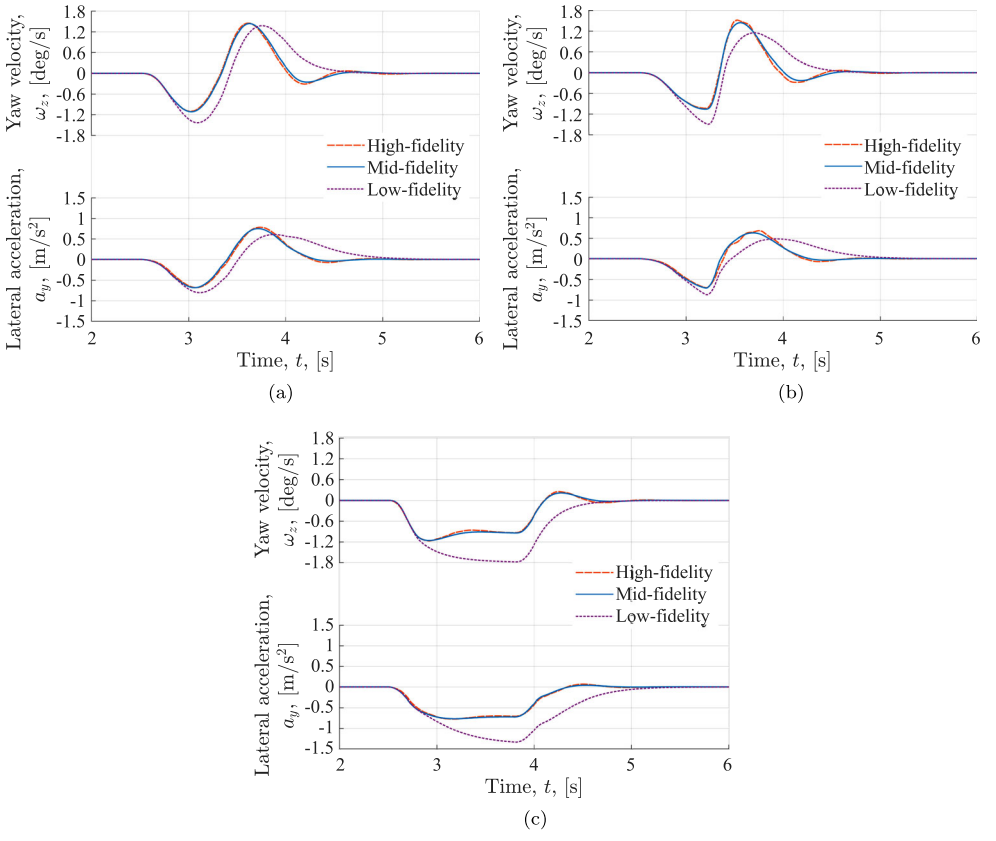

Figure 9. Fidelity analysis; comparing the yaw velocity and lateral acceleration response during the gust profiles, for the three vehicle dynamics models: (a) Profile 1, (b) Profile 2, (c) Profile 3.

dynamics model (high fidelity) was used as the reference. Evidently, the classical bicycle model (low fidelity) failed to emulate the response in terms of yaw velocity and lateral acceleration. Its response was slower with varying magnitude, acting as a too damped system. The enhanced model (mid fidelity) matched the response of the high-fidelity model well, proving that the essential system properties for this load case have been accurately implemented in this model. This fidelity analysis was also conducted to justify further use of the enhanced model in this study, including the parametric sensitivity analysis.

Experimental data from test track measurements [3] were used to validate the enhanced model. Thirteen instances associated with stability issues were selected. Vehicle-local wind measurement and the steering wheel angle were used as the input to the enhanced model. The modelled and measured yaw velocity and lateral acceleration response could then be compared. Figure 10 shows one of the instances. The model successfully captures the rapid changes and amplitude values in the measured data. All 13 instances were analysed, and Figure 11 compared the measured and modelled values of the combined measure (Equation 3). The diagonal line shows the ideal solution, where the modelled and measured values are equal. The data showed a fit of $R^2 = 0.83$ to the diagonal line, which was regarded acceptable considering the uncertainty of the measurement equipment and external disturbances (such as road unevenness) during the test track experiments. However, the model

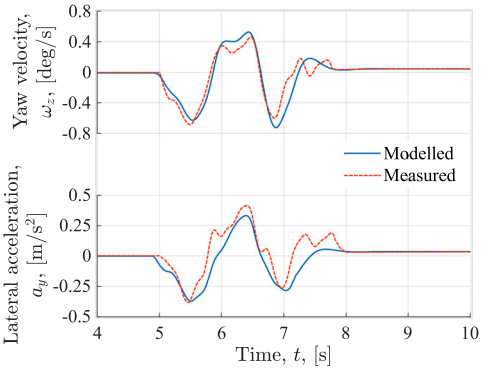

Figure 10. Validation of the enhanced (mid fidelity) model; comparing modelled versus measured yaw velocity and lateral acceleration response during crosswind gust event No. 8.

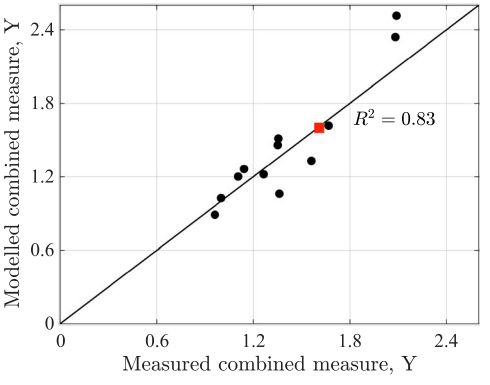

Figure 11. Measured vs. modelled values of the combined measure, Y (Equation (3)). The orange square corresponds to gust event No. 8, seen in Figure 10.

seemed to overpredict the response of the two strongest crosswind events. The highest driver steering wheel intervention was found at these events; hence, too simple modelling of the steering system could explain the overpredictions. Nevertheless, the parametric sensitivity study was performed using a fixed steering wheel angle, and the simplified steering system did not affect those results. The orange square data point represents the instance seen in Figure 10.

5.3. Parametric sensitivity study

5.3.1. Vehicle dynamic analysis

The first parametric analysis focused on vehicle dynamics. All 16 vehicle dynamic parameters were included while keeping the aerodynamic parameters at constant nominal values. Figure 12 shows the main effects of the significant parameters, where only 8 of the 16 parameters proved to be significant for any of the gust profiles. The longitudinal centre of gravity position (V4) had the highest main effect, based on the chosen parameter intervals. The positive effect of 0.85 (profile 1) indicates that increasing V4, i.e. moving the centre of gravity (CoG) rearwards, would increase the vehicle motion response to the crosswind,

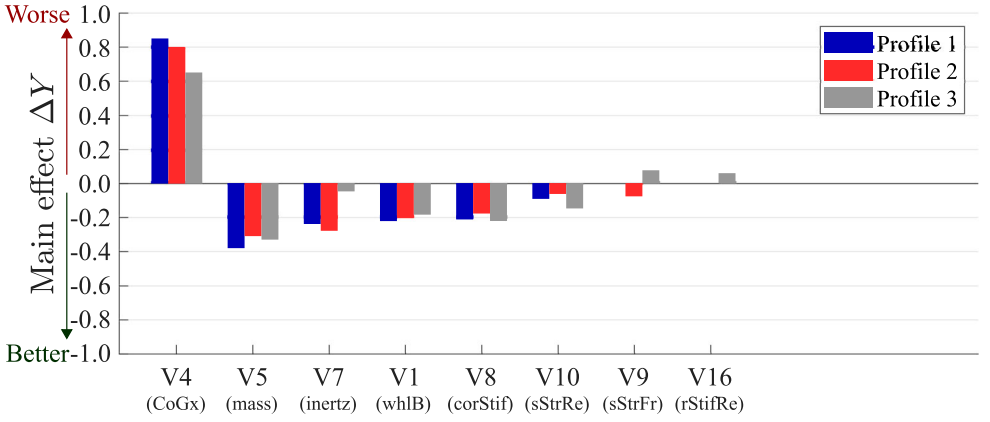

Figure 12. The main effects of the significant vehicle dynamic parameters.

and thus affect vehicle driving stability performance negatively. This effect was expected and have been seen in other studies [17,29,31,32]. In general, it could be noted that the trend effect of each parameter was persistent regardless of gust profile, although the magnitude and level of significance varied. To minimise the yaw velocity response, increasing vehicle mass (V5) and yaw moment of inertia (V7) proved to be beneficial. Figure 12 also demonstrates the importance of wheel base (V1), tire lateral cornering stiffness (V8) and finally, the rear and front axle side force steer gradient (V10 and V9) and the rear axle roll stiffness (V16). Even though V9, V10 and V16 had smaller main effects, it was regarded as an interesting finding since it showed that suspension characteristics have the potential to influence stability when primary vehicle parameters cannot be changed. This study of the main effects was a quite general investigation, and it was therefore complemented with the response surface methodology. The response surface analysis showed non-linear effects and interesting synergies between parameters.

The synergy between the front axle side force steer (V9) and roll steer (V11) was significant and can be seen in Figure 13. The magnitude of each parameter effect depends on the other parameter's value (i.e. a synergy effect). It is also evident from the figure that the effects were non-linear. The parameters must therefore be tuned simultaneously. Furthermore, these non-linearities proved to change depending on other parameter settings, e.g. V4 and height of CoG (V3). In summary, this shows the complexity of the vehicle dynamic system.

5.3.2. Aerodynamic analysis

The second analysis focused on the nine aerodynamic parameters, while keeping the vehicle dynamic parameters at constant nominal values. The significant main effects can be seen in Figure 14. It is evident that the aerodynamic yaw moment coefficient gradient (A9) had an effect comparable to the vehicle dynamic effect, V4, while the other two significant aerodynamic effects were smaller. The driving stability in crosswinds can thus be improved by flattening the yaw moment coefficient (C_{ym}) flow angle curve. This translates to moving the centre of pressure (CP) rearwards (Figure 1). The other significant parameters were the side force coefficient (A1) and the roll moment coefficient gradient (A8). Interestingly,

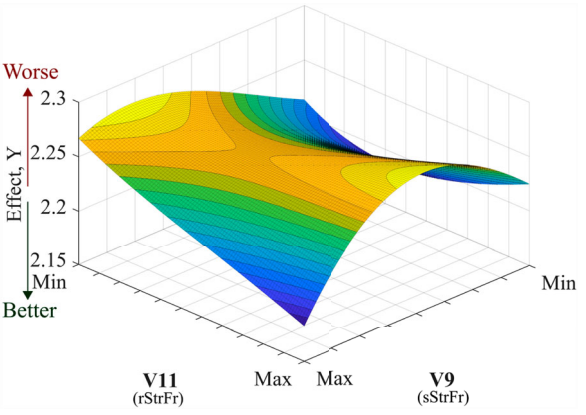

Figure 13. Visualisation of the synergy effect between parameters V9 and V11.

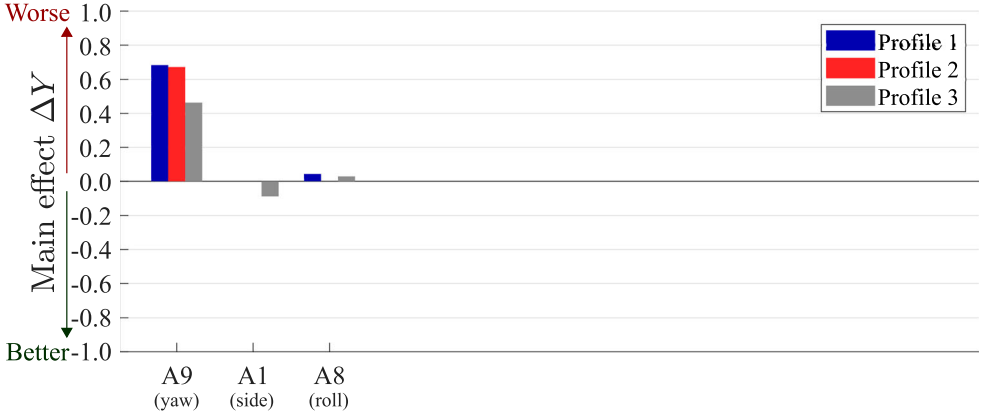

Figure 14. The main effects of the significant aerodynamic parameters.

the aerodynamic side force did not have a significant effect, except for gust profile 3 having a negative effect. Hence, increased side force gradient was, counter-intuitively, beneficial for profile 3. These results indicate that the yaw moment was the dominant quantify of the lateral aerodynamics.

It is noteworthy that none of the parameters controlling the lift coefficients (A4–A7) were significant, even though these are known to affect high speed stability [30]. The significance of the parameters is dependent on the chosen interval spread. Nevertheless, the intervals were based on realistic variations of different designs and vehicle types. Hence, the lift forces seem to be less important for crosswinds stability, if kept within typical values of modern passenger vehicles.

5.3.3. Combined analysis

The third analysis combined all vehicle dynamic and aerodynamic parameters into one parametric sensitivity study. The main effects of the significant parameters can be seen in Figure 15, where most significant parameters from the vehicle dynamic analysis (Figure

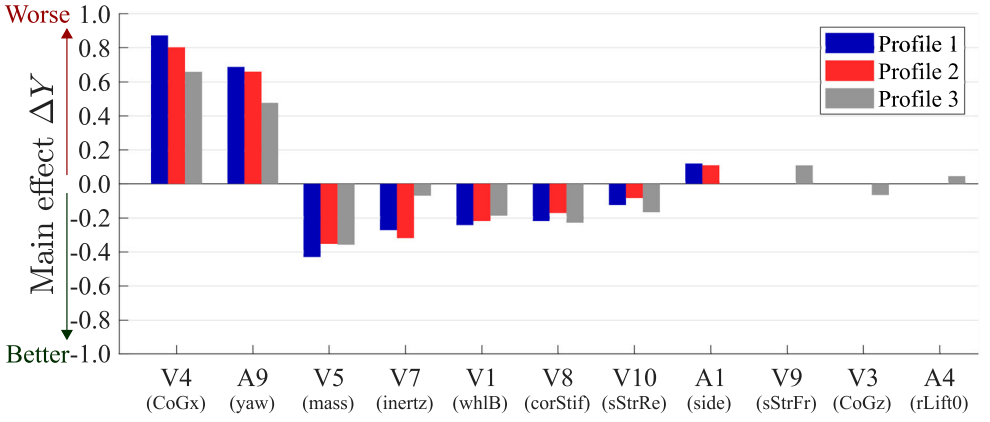

Figure 15. The main effects of the significant vehicle dynamic and aerodynamic parameters combined.

12) were included along with the aerodynamic yaw moment coefficient (A9), side force coefficient (A1) and rear axle lift coefficient (A4). The effects were similar in size in the combined analysis, as in the separate analyses, indicating low synergy between the most important parameters. The combined analysis also showed new significant parameters for profile 3, namely the CoG height (V3) and rear axle lift force (A4). Nevertheless, these parameters had small effects and the general recommendations for decreasing crosswind sensitivity are to move CoG forwards and reduce the aerodynamic yaw moment coefficient, if possible. Furthermore, it should be noted that increasing the vehicle mass (V5), which is negative for many vehicle attributes, would improve the straight-line driving stability performance during crosswinds.

5.3.4. Tire and wheel suspension analysis

Since many attributes need to be taken into consideration when designing a passenger vehicle, it might not be an alternative to alter the position of CoG, mass, wheel base or other primary vehicle parameters. Therefore, a fourth parametric analysis was conducted only focusing on suspension and tire parameters (V8–V16). The other vehicle dynamic and aerodynamic parameters were kept at constant nominal values. Four out of the seven parameters proved to have significant main effects, see Figure 16. The tire lateral cornering stiffness (V8) had the highest main effect where stiffer tires seemed to improve driving stability by lowering the vehicle response to crosswinds. The side force steer gradients at both axles (V9 and V10) were significant along with the roll steer gradient at the rear axle (V12), even though the effects were quite small.

The continued analysis including the response surface methodology revealed a significant synergy between the side force steer at the front and rear axle (V9 and V10), see Figure 17. Hence, setting requirements on the side force steer gradients should include a balanced view of both axles. It should also be noted that both the side force (V9–V10) and roll steer (V11–V12) showed non-linear effects and synergies between axles and each other, as seen in Figures 13 and 17. In summary, these results prove that it is possible to improve high speed driving stability without altering the primary vehicle dynamic parameters.

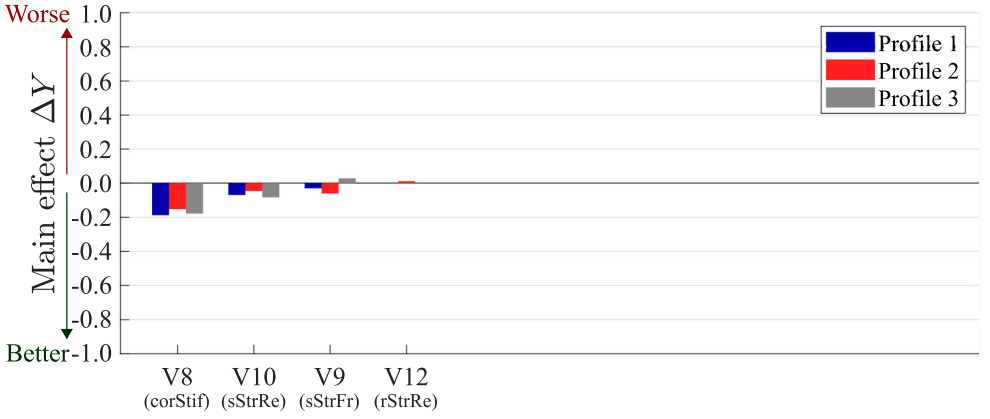

Figure 16. The main effects of the significant *realistic* vehicle dynamic parameters.

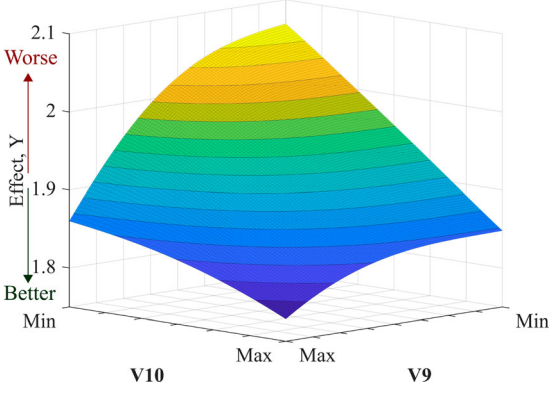

Figure 17. Visualisation of the synergy effect between parameters V9 and V10.

6. Conclusion

This paper introduced a combined vehicle dynamic and aerodynamic parametric sensitivity study with the purpose of finding key vehicle properties for minimising crosswind sensitivity. The study was carried out in a simulation environment, where the aerodynamic responses to the crosswind gusts were modelled using three approaches: two quasi-steady approaches (QS and QSD), where the last accounted for the time delay between the front and rear axle, and a transient CFD (tCFD) crosswind simulation methodology. The aerodynamic responses were one-way coupled to vehicle dynamic models of varying fidelity.

It was shown that the bicycle model (low-fidelity) could not estimate the response adequately, while the enhanced model (mid-fidelity) performed equivalently as the high-fidelity Adams/Car model. In agreement with previous work [17,29,31,32], the parametric study showed that centre of gravity (CoG) position was the most important parameter. Nonetheless, several other parameters had a high impact on crosswind stability, such as aerodynamic yaw moment coefficient, vehicle mass, wheelbase, side force steer coefficients,

and roll steer coefficients. Based on the finite set of parameters included in this study, the following conclusions could be drawn:

- The transient CFD crosswind simulations showed yaw moment overshoots when the flow angle changed rapidly. These overshoots could be modelled using a quasi-steady approach accounting for the time delay between the front and rear axle (QSD) when driving into crosswinds. No other significant transient fluid dynamic effect was found, and it could be concluded that the QSD approach was sufficient for approximating the aerodynamic response to crosswinds of the magnitude and frequency investigated in this study.
- The enhanced vehicle dynamic model could accurately capture the yaw velocity and lateral acceleration response to crosswinds, using the multi-body dynamic Adams/Car model as a reference. Furthermore, the enhanced model showed good agreement with the validation set of experimental test track data.
- The parametric sensitivity study proved that the longitudinal positioning of CoG (V4) has the largest influence on crosswind sensitivity, followed by the aerodynamic coefficient of yaw moment gradient (A9).
- Other significant vehicle dynamic characteristics were vehicle mass (V5), yaw mass moment of inertia (V7) and wheel base (V1). Increasing these parameters proved beneficial for crosswind stability.
- Both tire and suspension parameters pose realistic solutions for increasing crosswind stability performance. Increasing the lateral tire cornering stiffness (V8) proved beneficial, and the side force steer gradients at both the front axle (V9) and especially at the rear axle (V10) were found to be significant. The front axle side force steer (V9) showed a strong non-linear synergy with the roll steer (V11) and similarly with the rear axle side force steer (V10). Hence, the conclusion is that much can be done in the suspension setting to improve crosswind stability.

Disclosure statement

No potential conflict of interest was reported by the author(s).

ORCID

Adam Brandt http://orcid.org/0000-0002-1921-7694
Bengt Jacobson http://orcid.org/0000-0002-5798-5651
Simone Sebben http://orcid.org/0000-0002-7792-424X

References

[1] MacAdam CC, Sayers MW, Pointer JD, et al. Crosswind sensitivity of passenger cars and the influence of chassis and aerodynamic properties on driver preferences. Vehicle Syst Dyn. 1990;19(4):201–236. DOI:10.1080/00423119008968942
[2] Willumeit HP, Müller K, Dödlbacher G, et al. Method to correlate vehicular behaviour and driver's judgement under side wind disturbances. Vehicle System Dyn. 1988;17:508–524. DOI:10.1080/00423118808969292

[3] Brandt A, Sebben S, Jacobson B, et al. Quantitative high speed stability assessment of a sports utility vehicle and classification of wind gust profiles. SAE Technical Paper Series. 2020. DOI:10.4271/2020-01-0677
[4] Hucho WH. Aerodynamics of road vehicles. 4th ed. Warrendale (PA): Society of Automotive Engineers; 1998.
[5] Forbes DC, Page GJ, Passmore MA, et al. A fully coupled, 6 degree-of-freedom, aerodynamic and vehicle handling crosswind simulation using the drivaer model. SAE Int J Passenger Cars Mech Syst. 2016;9(2):710–722. DOI:10.4271/2016-01-1601
[6] Carbonne L, Winkler N, Efraimsson G. Use of full coupling of aerodynamics and vehicle dynamics for numerical simulation of the crosswind stability of ground vehicles. SAE Int J Commer Veh. 2016;9(2):359–370. DOI:10.4271/2016-01-8148
[7] Li SY, Gu ZQ, Huang TM, et al. Coupled analysis of vehicle stability in crosswind on low adhesion road. Int J Numer Methods Heat Fluid Flow. 2018;28(8):1956–1972. DOI:10.1108/hff-01-2018-0013
[8] Huang T, Li S, Wan Z, et al. Investigation of vehicle stability under crosswind conditions based on coupling methods. Proc Inst Mech Eng Part D J Autom Eng. 2019. DOI:10.1177/0954407018822424
[9] Sims-Williams D. Cross winds and transients: reality, simulation and effects. SAE Int J Passenger Cars Mech Syst. 2011;4(1):172–183. DOI:10.4271/2011-01-0172
[10] Cooper KR, Watkins S. The unsteady wind environment of road vehicles, part one: A review of the on-road turbulent wind environment. SAE Technical Paper Series. 2007. DOI:10.4271/2007-01-1236
[11] Wordley S, Saunders JW. On-road turbulence. SAE Int J Passeng Cars Mech Syst. 2008;1(1):341–360. DOI:10.4271/2008-01-0475
[12] Wordley S, Saunders JW. On-road turbulence: part 2. SAE Int J Passeng Cars Mech Syst. 2009;2(1):111–137. DOI:10.4271/2009-01-0002
[13] Fukagawa T, Shimokawa S, Itakura E, et al. Modeling of transient aerodynamic forces based on crosswind test. SAE Int J Passeng Cars Mech Syst. 2016;9(2):572–582. DOI:10.4271/2016-01-1577
[14] Nakasato K, Tsubokura M, Ikeda J, Onishi K, et al. Coupled 6dof motion and aerodynamic crosswind simulation incorporating driver model. SAE Int J Passeng Cars Mech Syst. 2017;10(2):662–670. DOI:10.4271/2017-01-1525
[15] Lewington N, Ohra-aho L, Lange O. The application of a one-way coupled aerodynamic and multi-body dynamics simulation process to predict vehicle response during a severe crosswind event. SAE Technical Paper Series. SAE International; 2017. DOI:10.4271/2017-01-1515
[16] ISO 12021:2010 Road vehicles 'Sensitivity to lateral wind' Open-loop test method using wind generator input. International Organization for Standardization. 2010.
[17] Tunay T, O'Reilly CJ, Drugge L. The significance of roll on the dynamics of ground vehicles subjected to crosswind gusts by two-way coupled simulation of aero- and vehicle dynamics. Advances in Dynamics of Vehicles on Roads and Tracks. 2020. p. 1388–1397. (Lecture Notes in Mechanical Engineering). DOI:10.1007/978-3-030-38077-9_160
[18] Wojciak J. Quantitative Analysis of Vehicle Aerodynamics during Crosswind Gusts[PhD Thesis]. Technical University of Munich; 2012.
[19] Theissen P. Unsteady Vehicle Aerodynamics in Gusty Crosswind[Phd thesis]. Technical University of Munich; 2012.
[20] Lawson AA, Sims-Williams DB, Dominy RG. Effects of on-road turbulence on vehicle surface pressures in the A-pillar region. SAE Int J Passenger Cars Mech Syst. 2009;1(1):333–340. DOI:10.4271/2008-01-0474
[21] Jarlmark J. Driver-vehicle interaction under influence of crosswind gust[Licentiate thesis]. Royal Institute of Technology; 2002.
[22] Klasson J. A generalised crosswind model for vehicle simulation purposes. Vehicle Syst Dyn. 2001;37:3114. DOI:10.1080/00423114.2002.11666245
[23] Juhlin M. Aerodynamic loads on buses due to crosswind gusts-on-road measurements. Vehicle Syst Dyn. 2008;46(sup1):827–835. DOI:10.1080/00423110802037081

[24] Drugge L, Juhlin M. Aerodynamic loads on buses due to crosswind gusts: extended analysis. Vehicle Syst Dyn. 2010;48(1sup):287–297. DOI:10.1080/00423111003739814
[25] Favre T. Aerodynamics simulations of ground vehicles in unsteady crosswind [PhD thesis]. Royal University of Technology; 2011.
[26] Nakashima T, Tsubokura M, Vázquez M, et al. Coupled analysis of unsteady aerodynamics and vehicle motion of a road vehicle in windy conditions. Comput Fluids. 2013;80:1–9. DOI:10.1016/j.compfluid.2012.09.028
[27] Chadwick A, Garry K, Howell J. Transient aerodynamic characteristics of simple vehicle shapes by the measurement of surface pressures. SAE Technical Paper Series. 2000. DOI:10.4271/2000-01-0876
[28] Huemer J, Stickel T, Sagan E, et al. Influence of unsteady aerodynamics on driving dynamics of passenger cars. Vehicle Syst Dyn. 2014;52(11):1470–1488. DOI:10.1080/00423114.2014.944-191
[29] Buchheim R, Maretzke J, Piatek R. The control of aerodynamic parameters influencing vehicle dynamics. SAE Paper. 1985. p. 850279–850279. DOI:10.4271/850279
[30] Howell J, Le Good G. The influence of aerodynamic lift on high speed stability. SAE Technical Paper SeriesTechnial. 1999;01(0651):8–8. DOI:10.4271/1999-01-0651
[31] Oraby WAH, Crolla DA. Passenger car stability under random wind excitation. SAE Technical Paper Series. SAE International, 2001. DOI:10.4271/2001-01-0133
[32] Juhlin M, Eriksson P. A vehicle parameter study on crosswind sensitivity of buses. SAE Technical Paper Series. 2004. DOI:10.4271/2004-01-2612
[33] Favre T, Näfver JJ, Jerrelind J, et al. Static coupling between detached-eddy simulations and vehicle dynamic simulations of a generic road vehicle model with different rear configurations in unsteady crosswind. Int J Veh Des. 2016;72(4):332. DOI:10.1504/IJVD.2016.082384
[34] Menter F. Stress-Blended Eddy Simulation (SBES)–A New Paradigm in Hybrid RANS-LES Modeling. Chapter 3, Notes on numerical fluid mechanics and multidisciplinary design. Springer International Publishing; 2018. ISBN 978-3-319-70030-4 978-3-319-70031-1. DOI:10.1007/978-3-319-70031-1_3
[35] Ekman P, Larsson T, Virdung T, et al. Accuracy and speed for scale-resolving simulations of the drivaer reference model. SAE Technical Paper Series. 2019. DOI:10.4271/2019-01-0639.
[36] Kuiper E, Van Oosten JJM. The PAC2002 advanced handling tire model. Veh Syst Dyn. 2007;45(sup1):153–167. DOI:10.1080/00423110701773893